The Interaction of an Eddy with an Unstable Jet

GEORGE I. BELL AND LARRY J. PRATT

Woods Hole Oceanographic Institution, Woods Hole, Massachusetts

(Manuscript received 5 December 1990, in final form 18 October 1991)

ABSTRACT

Interactions between an unstable jet and eddy are explored using a jet with piecewise constant potential vorticity. A linear theory is developed for the case where the jet is nearly zonal and the eddy is far away in the sense that the eddy may be replaced by a point vortex that induces velocity perturbations in the jet small compared with the maximum jet velocity. The calculations are extended into the nonlinear domain by the method of contour dynamics. Specific examples of barotropic and equivalent barotropic jets are discussed, with particular attention to processes leading to eddy propagation.

In the barotropic case, long-range eddy–jet interactions are dominated by the jet instability, which breaks the jet up into eddies downstream from the forcing eddy. For a forcing eddy south of an unperturbed eastward flowing jet, the initial eddy propagation tendency is southwestward (SW) for cyclones and northeastward (NE) for anticyclones. In the equivalent barotropic case, the fact that long waves in the jet are neutrally stable modifies the interaction considerably. The instability triggered by the eddy may be advected downstream rapidly enough that it does not affect the eddy. A long wavelength, steady lee wave may develop downstream from the forcing eddy, and this results in a propagation of the eddy in the opposite direction from the barotropic case (NE for cyclones, SW for anticyclones).

Short-range interactions tend to be strongly nonlinear and can result in stripping of fluid from the edge of the jet. The detached fluid and eddy can then propagate as a vortex pair away from the jet, and the whole process therefore inhibits absorption of eddies by the jet. Some Gulf Stream warm outbreaks may result from such interactions.

1. Introduction

Gulf Stream rings originate from pinched off meanders of the Gulf Stream and are among the most energetic eddies in the world oceans. Once separated from the stream, rings follow varied and complicated trajectories (Richardson 1983). The drift of a Gulf Stream ring may be attributed to a variety of physical effects. First, it will be advected by the large-scale flow that surrounds it, such as the recirculation regions of the Gulf Stream. Second, the ring may be constrained by large topographic features, such as the continental shelf. Third, if the eddy is axially asymmetric (Smith and Bird 1989) or has a baroclinic structure (Hogg and Stommel 1985), this may induce self propagation. Finally, the ring may interact with the potential vorticity distribution that surrounds it, resulting in a drift. For example, it may interact with the background planetary vorticity gradient (Nof 1981; McWilliams and Flierl 1979), nearby rings, or the Gulf Stream itself. All of these effects contribute to some extent to the motion of Gulf Stream rings, and at any given time a combination of several effects are likely responsible for the observed motion of a ring.

Corresponding author address: Dr. George I. Bell, US West Advanced Technologies, 4001 Discovery Dr., Suite 270, Boulder, CO 80303.

In this paper we concentrate on eddy propagation due to interactions with the potential vorticity field of a neighboring jet. In the majority of cases we will represent the eddy by a point vortex and the jet by a band of potential vorticity fronts (in cases where the eddy nears the jet, we will represent it by a patch of constant potential vorticity).

Stern and Flierl (1987), hereafter abbreviated SF, suggested a simple and intuitive mechanism for meridional eddy propagation due to interaction with a jet. In Fig. 1, we show an eddy interacting with the edge of a barotropic shear layer (such a shear-layer edge, across which the potential vorticity jumps discontinuously, will be called a contour). The eddy advects the contour away from its zonal alignment, and the potential vorticity anomalies created in the jet in turn induce a meridional drift of the eddy. In an analogous fashion, an anticyclonic eddy would be convected toward the shear layer.

The jet considered by SF was stable and symmetric. Because jets arising in geophysical settings are typically unstable and often asymmetric, it would appear useful to understand how these additional elements alter the dynamics of eddy–jet interactions. The calculations presented herein are attempts to quantify the eddy drift direction and describe the qualitative phenomena occurring in several idealized jet models. In particular, we concentrate on one barotropic and one equivalent

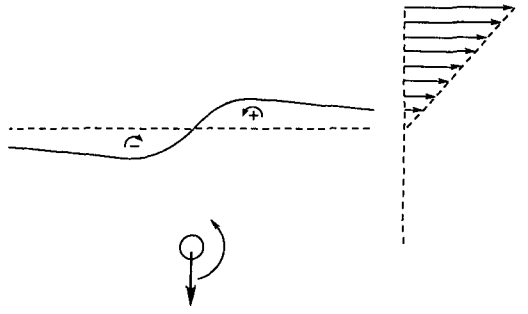

FIG. 1. A cyclonic eddy interacting with an anticyclonic shear layer. The shear-layer edge (or contour) is initially aligned zonally, resulting in the velocity profile shown on the right. As the eddy advects the contour around itself, the vorticity anomalies induced advect the eddy away from the shear layer.

barotropic jet, each having the simplest possible unstable potential vorticity distribution. A piecewise uniform potential vorticity distribution allows one to construct a simple linear theory to predict the initial motion of the eddy toward or away from the jet. Nonlinearities associated with the growth of unstable waves in the jet and the movement of the eddy close to the jet are beyond the scope of the linear theory, and numerical solutions are required to determine whether initial tendencies persist.

The jets considered are not posed as Gulf Stream models but, rather, as flows having certain elements in common with geophysical jets. The first example is a barotropic triangular jet composed of four regions of uniform vorticity (Fig. 2a). When perturbed at the most unstable wavelength, this jet breaks up into a vortex street (see Fig. 7). Although not particularly relevant to the Gulf Stream, the triangular jet is a direct extension of previously studied barotropic shear flows (SF; Bell 1990), and may be relevant for other geophysical jets.

The second case considered (Fig. 2b) is that of an equivalent barotropic jet that is unstable as well as nonsymmetric meridionally. Such a jet has been used previously in connection with the study of the formation process of eddies known as Gulf Stream warm outbreaks (Pratt et al. 1990). When perturbed, this jet meanders and sheds eddies but does not break up into isolated eddies as does the triangular jet.

An eddy interacting with an initially zonal triangular jet is depicted in Fig. 3. When the basic shear flow is unstable the direction of meridional drift of an interacting eddy is not as obvious as in Fig. 1. While the perturbations to the outer interfaces induce southward propagation of the eddy, the middle interface (twice as strong) induces northward propagation. In addition, because the jet itself is unstable, we expect it to begin to break up as the interaction proceeds.

It is useful to introduce a notation for the sign of an eddy relative to the side of the jet that it lies on. Ikeda and Apel (1981) referred to an eddy that was opposite in sign to a Gulf Stream ring as an *opposite* eddy. Following this convention, an eddy will be referred to as a regular eddy if the velocity field it induces at the jet opposes the flow of the jet. Both cold core rings (cyclonic) to the south of the Gulf Stream and warm core rings (anticyclonic) to its north are regular eddies. An eddy that is not a regular eddy will be referred to as an "opposite" eddy (anticyclone south of Gulf Stream, or cyclone north of it). A "warm outbreak" is an example of an opposite eddy. Note that some jets, such as the triangular jet, tend to break up into opposite eddies, while meandering jets, such as the Gulf Stream, tend to pinch off regular eddies (Gulf Stream rings).

In section 2 the equations of motion for the jet and point vortex are presented. A linear theory valid for long-range eddy–jet interactions is given in section 3. In this linear theory, changing the sign of the forcing eddy merely reverses the sign of the contour displacements and the eddy propagation direction. When the eddy is near a jet, their interaction is nonlinear, and in section 4, we argue that fundamentally different phenomena are expected for cyclonic versus anticyclonic eddies based on the location of stagnation points in the flow. A generalized expression for the meridional eddy drift rate, valid for arbitrarily large displacements of the contours, is also presented in section 4.

Sections 5 and 6 present numerical results for barotropic and equivalent barotropic cases, respectively. In short, we focus on the physical processes leading to propagation of the forcing eddy and the differences between the two cases. In the barotropic case, we will show that no long resonant waves exist and that the drift of the eddy is due entirely to unstable waves.

In the equivalent barotropic case resonant waves are

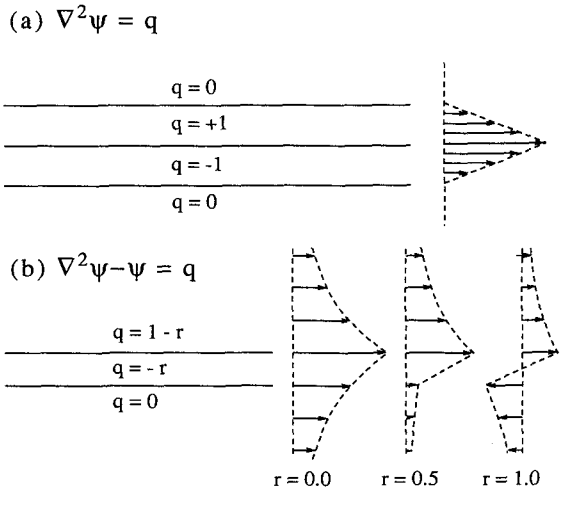

FIG. 2. Unperturbed potential vorticity distribution and velocity profiles of two unstable jets: (a) the barotropic triangular jet and (b) an equivalent barotropic jet ($-r$ denotes the potential vorticity jump across the southern contour).

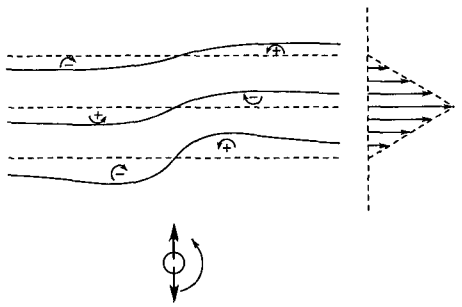

FIG. 3. A cyclonic eddy interacting with a triangular jet. The vorticity anomalies induced do not sum to give an obvious meridional propagation direction (compare with Fig. 1).

present, and they completely change the nature of the interaction. Unstable waves are often advected so far downstream that their interaction with the jet is negligible compared with the resonant waves. Just downstream of the eddy, a standing lee resonant wave forms, leading to eddy propagation directions opposite that of the barotropic case. In section 7 we discuss the long-wave properties of barotropic and equivalent barotropic jets and suggest that these properties control how that jet interacts with distant eddies.

A nonlinear phenomenon shared by both types of jets is the stripping away of opposite-signed vorticity by a nearby regular eddy. This stripped-off vortex and eddy advect one another away from the jet as a dipole structure. In section 8 we argue that this stripping process is analogous to the formation of warm outbreaks in the Gulf Stream by cold core rings.

2. Equations of motion

We consider a model in which the jet is represented by n initially parallel potential vorticity discontinuities (contours), with y coordinates a_j, as depicted in Fig. 4. The potential vorticity jump across the jth contour is Δ_j, and the deviation of the contour from its undisturbed position $y = a_j$ is denoted $L_j(x, t)$. Our convention (opposite that of SF) is that a positive Δ_j corresponds to an increase in potential vorticity as y increases. The eddy is represented by a point vortex located at $x_p(t)$, $y_p(t)$ (later, we will relax this to include patches of constant potential vorticity). We move into a reference frame translating uniformly with the initial drift speed of the point vortex, c. We choose the origin of our coordinate system so that (initially) $y = 0$ is at the point of maximum velocity of the jet, and the point vortex lies on the line $x = 0$, that is, $x_p(0) = 0$.

Length and time scales for the problem are determined as follows: we choose as our length scale l some measure of the jet width (in contrast to SF, who chose a length scale based on the point vortex circulation Γ). We define a time scale based on the maximum magnitude (Ω) of the potential vorticity in the jet. Thus, we scale distance by l, time by Ω^{-1}, velocity by $l\Omega$, and streamfunction and circulation by $l^2\Omega$. In nondimensional variables, the streamfunction for the flow is determined from the potential vorticity distribution q by

$$[\nabla^2 - \gamma^2]\psi = q = \sum_{j=1}^{n} \Delta_j H(y + L_j(x, t) - a_j) + \Gamma\delta(x - x_p)\delta(y - y_p), \quad (1)$$

where Γ is the circulation of the point potential vorticity vortex; $H(x)$ is the Heaviside step function, equal to 1 for $x > 0$ and 0 for $x \leq 0$; and $\delta(x)$ is the Dirac delta function. The parameter γ is the (dimensionless) inverse deformation radius, defined by

$$\gamma \equiv \frac{f_0 l}{(g'D)^{1/2}},$$

where f_0 is the effective Coriolis parameter, g' the reduced gravity, and D is the reference layer depth at $y = -\infty$. Note that by defining D in this fashion the potential vorticity south of the jet is zero.

Since q is advectively conserved, the motion of each contour and the point vortex (in the uniformly translating frame of reference) is given by

$$\left[\frac{\partial}{\partial t} - c\frac{\partial}{\partial x}\right]L_j = \frac{d}{dx}[\psi(x, a_j + L_j(x, t), t)] \quad (2)$$

$$\frac{\partial x_p}{\partial t} = -\frac{\partial \psi}{\partial y}(x_p, y_p, t) - c \quad (3)$$

$$\frac{\partial y_p}{\partial t} = \frac{\partial \psi}{\partial x}(x_p, y_p, t). \quad (4)$$

Following SF, we split the streamfunction into three parts: $\Psi(y)$, the streamfunction of the undisturbed flow; ψ', the contribution due to the perturbations of the contours; and ψ_p, the streamfunction of the point vortex:

$$\left[\frac{\partial^2}{\partial y^2} - \gamma^2\right]\Psi = \sum_{j=1}^{n} \Delta_j H(y - a_j) \quad (5)$$

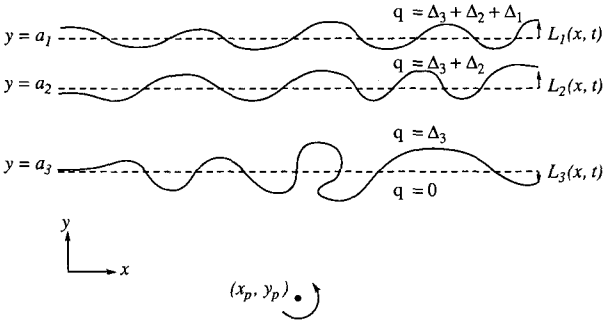

FIG. 4. A perturbed shear layer with piecewise constant potential vorticity.

$$[\nabla^2 - \gamma^2]\psi' = \sum_{j=1}^{n} \Delta_j[H(y + L_j(x, t) - a_j) - H(y - a_j)] \quad (6)$$

$$[\nabla^2 - \gamma^2]\psi_p = \Gamma\delta(x - x_p)\delta(y - y_p). \quad (7)$$

Associated with each streamfunction is a velocity field, denoted by $(U, 0)$, (u', v'), and (u_p, v_p), respectively. Note that by definition

$$c = -\Psi_y(y_p(0)) = U(y_p(0)). \quad (8)$$

Using the split streamfunction, the equations of motion (2)–(4) may be rewritten

$$\frac{\partial L_j}{\partial t} = v'(x, a_j + L_j, t) + v_p(x, a_j + L_j, t) - \frac{\partial L_j}{\partial x}[U(a_j + L_j) + u'(x, a_j + L_j, t) + u_p(x, a_j + L_j, t) - c] \quad (9)$$

$$\frac{\partial x_p}{\partial t} = u'(x_p, y_p, t) + U(y_p) - c \quad (10)$$

$$\frac{\partial y_p}{\partial t} = v'(x_p, y_p, t). \quad (11)$$

By integrating the Green's function for the operator $\nabla^2 - \gamma^2$ over the perturbation potential vorticity, we may invert (6) and (7). From such an integral representation of the streamfunctions ψ' and ψ_p, the advecting velocities are determined by differentiation. For the point vortex,

$$\psi_p = -\frac{\Gamma}{2\pi} K_0(\gamma[(x - x_p)^2 + (y - y_p)^2]^{1/2}),$$

where K_0 is the modified Bessel function or order zero. For the flow field induced by the contour displacements,

$$\psi'(x, y, t) = \frac{1}{2\pi} \sum_{j=1}^{n} \Delta_j \int_{-\infty}^{\infty} \int_{0}^{L_j(x',t)} K_0(\gamma[(x - x')^2 + (y - y')^2]^{1/2}) dy' dx'. \quad (12)$$

By applying Green's identity in the plane to (12), the associated velocity field may be written in terms of integrals over the contours L_j (see Polvani 1988). The nonlinear calculations in sections 5 and 6 were obtained by making minor modifications to existing contour dynamics programs. The codes used and their modifications are summarized in appendix B.

3. Linear theory

The basic assumption of the linear theory is that $|L_j| \ll 1$. In dimensional terms, the displacements of the contours that form the jet must be much less than the jet width and the characteristic wavelength of the displacement. Let d be the distance between the point vortex and closest contour at $t = 0$. We define

$$\epsilon = \left|\frac{u_p(0, d)}{U(0)}\right|, \quad (13)$$

where ϵ is the ratio of the maximum eddy-induced velocity at the jet to the maximum unperturbed jet velocity. If $\epsilon \gg 1$, then the eddy is stronger than the jet and will tend to wind the jet around itself. When $\epsilon \ll 1$, the jet is robust and its structure persists: we will refer to such an interaction as a weak interaction.

If the jet is stable and $\epsilon \ll 1$, then the first two terms on the right-hand side of (9) will balance and (to leading order) the contour amplitudes will remain $O(\epsilon)$ for all time (as in SF and Bell 1990). However, since the basic jets we are considering are themselves unstable, the linear solution will always break down in finite time.

Assuming $\epsilon \ll 1$, then u_p and v_p evaluated at any point in the jet are $O(\epsilon)$. If we assume $L_j = O(\epsilon)$ initially, then the perturbing velocities due to contour deformations, u' and v', are $O(\epsilon)$ everywhere. The linearized versions of the jet evolution equation (9), the perturbation streamfunction (6), and the point vortex streamfunction (7) are

$$\frac{\partial L_j}{\partial t} = \frac{\partial \psi'}{\partial x}(x, a_j, t) + \frac{\partial \psi_p}{\partial x}(x, a_j) - \frac{\partial L_j}{\partial x}[U(a_j) - c] \quad (14)$$

$$[\nabla^2 - \gamma^2]\psi' = -\sum_{j=1}^{n} \Delta_j \delta(y - a_j) L_j \quad (15)$$

$$[\nabla^2 - \gamma^2]\psi_p = \Gamma\delta(x)\delta(y - y_p(0)). \quad (16)$$

Following SF and Bell (1990), we take the Fourier transform (with respect to x) of (14). We define

$$\hat{L}_j(k) \equiv \int_{-\infty}^{\infty} L_j(x) e^{-ikx} dx$$

and $\hat{\mathbf{L}}$ as the column vector with components $\hat{L}_j$. The system of linear ODEs that results may be compactly written

$$\frac{\partial \hat{\mathbf{L}}}{\partial t} + ik(\mathbf{A} - c\mathbf{I})\hat{\mathbf{L}} = ik\hat{\mathbf{f}}, \quad (17)$$

where the column vector $\hat{\mathbf{f}}(k)$ represents the point vortex forcing, the matrix $\mathbf{A}(k)$ embodies the linear stability properties of the jet, and $\mathbf{I}$ is the n by n identity matrix (see appendix A for detailed definitions of $\hat{\mathbf{f}}$ and $\mathbf{A}$).

The solution to the system of linear ODEs (17) may be represented conveniently in terms of exponentials of matrices (definition in appendix A). Using this no-

tation, the solution to (17) has exactly the same form as if $\hat{\mathbf{L}}$ and $\mathbf{A} - c\mathbf{I}$ were scalars,

$$\hat{L}(k, t) = \exp[-ik(\mathbf{A} - c\mathbf{I})t]\hat{\mathbf{L}}(k, 0)$$

evolution of initial condition

$$- (\mathbf{A} - c\mathbf{I})^{-1} \exp[-ik(\mathbf{A} - c\mathbf{I})t]\hat{\mathbf{f}}(k)$$

response due to eddy forcing

$$+ (\mathbf{A} - c\mathbf{I})^{-1}\hat{\mathbf{f}}(k) \quad \text{steady solution.} \quad (18)$$

To see why the matrix $\mathbf{A}$ embodies the linear stability properties of the jet alone, consider the more standard approach for determining linear jet stability. To do this, we remove the point vortex ($\hat{\mathbf{f}} = 0$) and let

$$L_j(x, t) = b_j e^{ik'(x-\omega t)}. \quad (19)$$

Substitution of (19) into (14) results in a solvability condition, which is that $\mathbf{b}$ (as a column vector) must be an eigenvector of $\mathbf{A}(k')$ with eigenvalue ω. To obtain (19) using (18), substitute in $\hat{\mathbf{L}}(k, 0) = \mathbf{b}\delta(k - k')$, $\hat{\mathbf{f}}(k) = 0$ and $c = 0$ to get

$$\hat{\mathbf{L}}(k, t) = e^{-ik\mathbf{A}t}\mathbf{b}\delta(k - k') = e^{-ik\omega t}\mathbf{b}\delta(k - k'). \quad (29)$$

The last equality holds because if $\mathbf{b}$ is an eigenvector of $\mathbf{A}$ with eigenvalue ω, then $\mathbf{b}$ is an eigenvector of $e^{\alpha\mathbf{A}}$ with eigenvalue $e^{\alpha\omega}$. We see that (20) is exactly the assumed form in (19). Thus, the first term on the right-hand side of (18) is the linear response of the jet to the initial condition. The second term is the response generated by eddy forcing, while the third term is a steady solution to (17).

From the form of (18), it is apparent that there are two types of waves that are important to the long-term evolution of the system. First, unstable waves have wavenumbers k_u such that $\mathbf{A}(k_u)$ has complex eigenvalues. The existence of an unstable wave implies that small disturbances in L grow exponentially with time. The phase speed of unstable waves is generally larger than the drift speed of the point vortex. Thus, they tend to drift downstream while growing to reach finite amplitude. In some cases unstable waves may drift downstream rapidly enough that they are unable to influence the eddy.

Second, resonant wavenumbers k_r are those for which $\mathbf{A}(k_r) - c\mathbf{I}$ fails to be invertible. Physically these correspond to neutral waves that drift at the same speed as the forcing eddy. In appendix A it is shown that for t large a resonant wavenumber k_r results in a linear growth of $|\hat{L}_j(k_r, t)|$ with time. Such linear growth, as we shall see, corresponds not to a linear growth in the actual contour amplitude but rather a downstream spreading of the resonant wave.

It is interesting to note that an unstable wave can never be a resonant wave. The forcing induces perturbations in the contours that are in phase, while unstable waves must be phase shifted relative to one another, a feature necessary for the extraction of kinetic energy from the flow by the disturbance (Pratt and Pedlosky 1990). Therefore, an unstable wave with phase speed c will grow exponentially by itself, but cannot grow at the expense of the eddy–jet separation, as is the case for a resonant wave.

Both unstable and resonant waves can induce meridional eddy drift, but by rather different mechanisms. Unstable waves induce meridional eddy drift when they grow to finite amplitude, *provided* they reach finite amplitude close enough to the eddy. On the other hand, a resonant wave induces meridional drifting completely within the framework of the linear theory. We can produce a formula for the direction of meridional drift resulting from the creation of a resonant wave. In appendix A, we derive the formula

$$\Gamma \frac{\partial y_p}{\partial t} \propto \sum_{j=1,n} \Delta_j |b_j(k_r)|^2, \quad (21)$$

where k_r is the resonant wavenumber and $\mathbf{b}(k_r)$ is the eigenvector of $\mathbf{A}(k_r)$ with eigenvalue c. Note that (21) specifies that by knowing the form of the resonant wave, we may calculate the *direction* of meridional eddy drift that the formation of the lee wave induces.

4. Nonlinear theory

Conservation of the x component of perturbed momentum $\partial\psi'/\partial y$ for the system (9)–(11) leads to the exact identity (see Bell 1990; Bell and Pratt 1993),

$$\Gamma \frac{\partial y_p}{\partial t} = \frac{1}{2}\frac{\partial}{\partial t}\left\{\sum_{j=1,n} \Delta_j \int_{-\infty}^{\infty} [L_j(x, t)]^2 dx\right\}, \quad (22)$$

where the integrals are interpreted as contour integrals over the contours L_j. This result was first derived by Bell (1990) for the case of a single contour. For a single contour, the sum in (22) contains only one term and the integral on the right-hand side is positive and should increase as the perturbations due to the eddy disperse along the contour. Thus, a definite direction of meridional drift is specified (toward or away from the jet) even when the interaction is highly nonlinear. The jets considered here are unstable and are composed of multiple contours with Δ_j of both signs. The momentum conservation law (22) remains valid but does not specify a single direction of meridional drift as the contours deform. Nonetheless, it is useful in understanding meridional drifting.

A simple kinematic argument can also give qualitative information about eddy–jet interactions. Polvani et al. (1989) were able to predict the filamentation of an elliptical vortex by tracking the location of a stagnation point in the flow. We use an analogous argument here to predict filamentation in the jet contour nearest the eddy. Suppose we move into a reference frame drifting zonally at the same speed as the eddy. Provided the jet is stronger than the eddy in the sense

that $\epsilon < 1$, there is always a stagnation point in the flow between a regular eddy and the jet (at this point the fluid velocity is identically zero in this reference frame). This situation is depicted in Fig. 5a, where we show streamlines for an eastward jet and regular (cyclonic, $\Gamma = 0.75$) eddy. In contrast, streamlines for the same jet with an opposite (anticyclonic) eddy of the same strength and in the same location are shown in Fig. 5b, and there is no stagnation point between the jet and eddy.

In Fig. 5, the shaded regions denote fluid particles inside the jet that lie on streamlines that eventually pass to the south of the eddy. Note that in the case of a regular eddy, more than half of the incoming jet lies in this region, while for the opposite eddy none of the incoming jet lies in this region. If the flow were steady, all the fluid particles entering from the left into the shaded region would be diverted around the eddy. While the pattern of streamlines changes radically as the flow evolves and the stagnation point moves as well, fluid that is always between the eddy and the stagnation point is destined to circulate south of the eddy rather than pass to the north of the eddy in the jet. We anticipate that when a stagnation point lies inside the jet for a significant percentage of an eddy turnover time, a regular eddy may strip off potential vorticity from the near edge of the jet. Being regular eddies, Gulf Stream rings may induce such a stripping phenomenon. Indeed, the relation of stripped regions and Gulf Stream warm outbreaks will be discussed in section 8.

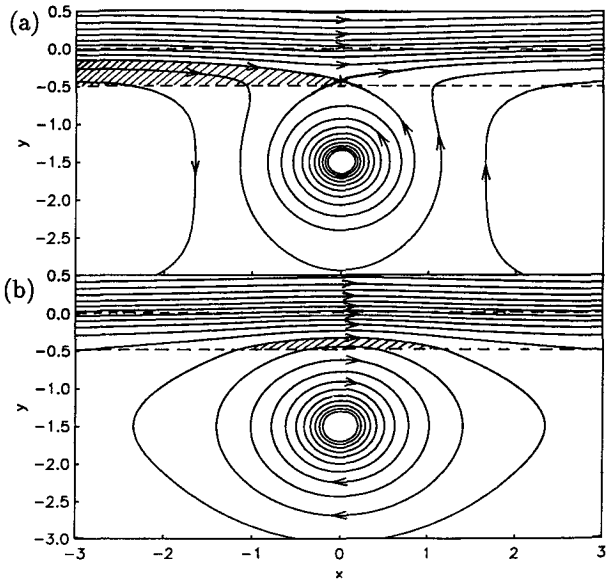

FIG. 5. Streamlines of an eddy interacting with the jet of Fig. 2b, in the frame of reference translating with the eddy (solid lines are streamlines, dotted lines are contours). (a) Regular (cyclonic) eddy; note stagnation point (parameters of Fig. 17). (b) Opposite (anticyclonic) eddy.

5. The triangular jet

The triangular jet (Fig. 2a) is the simplest symmetric barotropic jet (composed of contours). The dimensional jet width is $2l$, and the undisturbed flow is

$$U(y) = \begin{cases} 0, & \text{for } |y| \geq 1 \\ 1 - |y|, & \text{for } |y| \leq 1. \end{cases}$$

For an eddy outside an unperturbed jet, note that the initial eddy drift velocity c is always zero.

This jet is a special case of the type studied by Drazin and Howard (1962). Figure 6 shows the dispersion relation (the eigenvalues ω of $\mathbf{A}$ versus k). The neutrally stable symmetric mode is characterized by $L_2 = 0$ and $L_1 = -L_3$. Since the eddy tends to force interface displacements that are in phase, no resonance with this mode occurs. Also shown in Fig. 6 is an unstable mode with a short-wave cutoff (near $k = 1.8$) but no long-wave cutoff.

Nonlinear calculations of the triangular jet were performed by a contour dynamics code (see appendix B for the details). When the fastest growing wave ($k = k_u = 1.224$) is used as an initial condition (Fig. 7) the jet rolls up into a train of eddies of alternating sign (a vortex street). In our terminology, these eddies are all opposite eddies because of their sign and location relative to the original center of the jet. Pozrikidis and Higdon (1987) have considered the nonlinear evolution of unstable modes in an asymmetric triangular jet, and show that the wake structure varies considerably both in the location and number of the wake eddies.

Because the initial zonal drift speed of the point vortex is zero, a resonant wave must be a neutrally stable *stationary* wave. From Fig. 6 we see that there are no stationary neutral waves (except for a mode that displaces an entire contour uniformly, $k = 0$). Thus, there are no resonant waves in this eddy–jet interaction. We can anticipate that the dominant interaction will be that between the finite-amplitude unstable waves and eddy.

Suppose we begin with an unperturbed jet, $L_j(x, 0) = 0$. Figure 8 shows the prediction of the linear theory (18) for the Fourier amplitude of the middle contour, for $\Gamma = -2$ and $y_p(0) = -4$. That the spectrum of Fig. 8 is always dominated by waves with wavenumber less than k_u indicates that as nonlinearities become important, the dominant wavenumber of the spectrum will be less than that of the most unstable mode. The fully nonlinear simulation (Fig. 9) shows the development of a vortex street downstream from the eddy with a period greater than that of the most unstable mode. The spacing of the resultant eddies is $1.3\lambda_u$, where $\lambda_u = 5.133$ is the wavelength of the most unstable mode (1.3 was arrived at by averaging the distances between eddy centers).

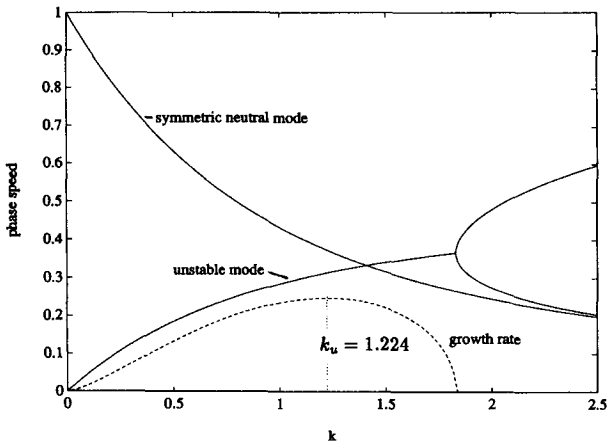

FIG. 6. The dispersion relationship for the barotropic triangular jet; k_u is the wavenumber of the fastest growing unstable wave.

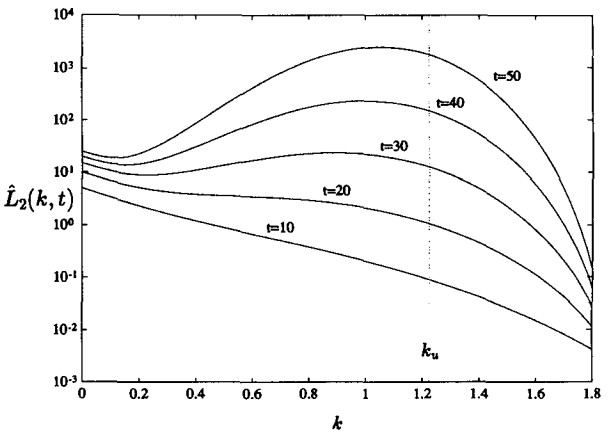

FIG. 8. The linear prediction of the Fourier transform of the middle contour of the triangular jet with $\hat{L}_j(k, 0) = 0$, $\Gamma = -2$, and $y_p(0) = -4$. Note that the spectrum is dominated by waves with $k < k_u$.

A similar shifting of the dominant wavelength of the instability due to eddy forcing has been observed by Ikeda and Lygre (1989). They attributed the shift to changes in the zonal eddy drift speed. (As c increases, the eddy forces the most unstable wave more strongly, and the dominant wavelength of the instability decreases.) In this case, a similar shift results from the fact that the eddy forces wavelengths longer than the most unstable mode preferentially. If the eddy was initially farther from the jet than in Fig. 9, the wake eddy spacing would be even larger (see Table 1).

By Fourier transforming the middle contour of Fig. 9 (at least when it is single valued) and comparing with Fig. 8, we may test the validity of the linear theory. The relative error,

$$\frac{\| L_2^{\text{exact}} - L_2^{\text{linear}} \|^2}{\| L_2^{\text{exact}} \|^2}, \tag{23}$$

where $\| f \|^2 \equiv \int_0^L [f(x)]^2 dx$ increases more or less exponentially with time from 10^{-5} at $t = 0$ to 10^{-2} at $t = 20$).

The linear theory may be invoked to calculate the initial meridional propagation velocity of the eddy starting from an initially zonal jet. According to (41), Γ and $\partial y_p / \partial t$ have opposite signs. Thus, regular eddies initially propagate away from the jet, while opposite eddies propagate toward the jet. This direction is in agreement with the calculations of SF and (21), where only a single contour representing the near edge of the jet is used.

Further study shows that the wake pattern, as well as the eddy drift, is quite sensitive to the initial conditions. For example, suppose we start using the parameters of Fig. 9 but for the initial jet use the linear steady solution in (18). The simulation (no figure)

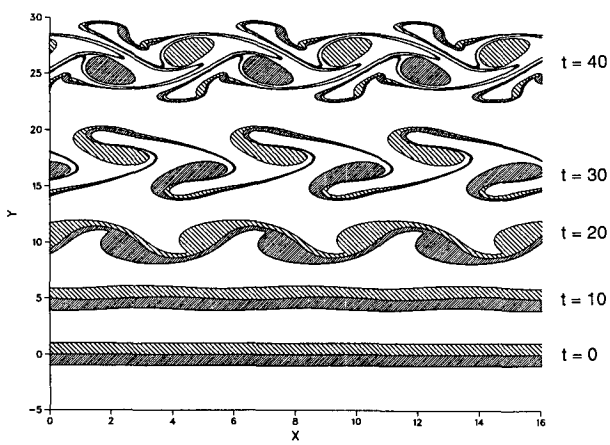

FIG. 7. The nonlinear development of the most unstable wave, $k_u = 1.224$, initial amplitude $|L_1| = 0.01$, showing the formation of a vortex street.

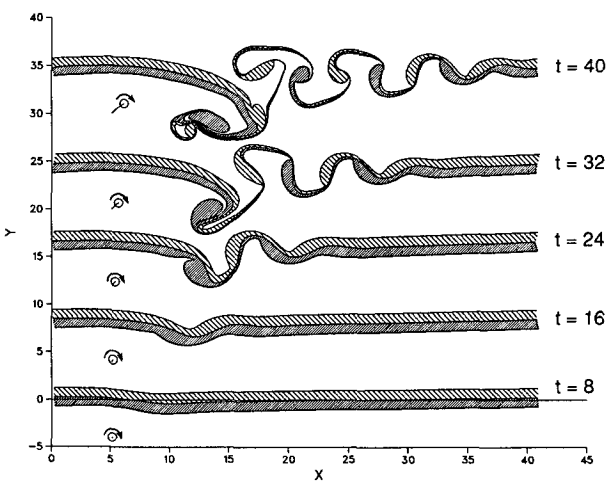

FIG. 9. Contour dynamics simulation of an eddy interacting with an initially zonal jet, with the same parameters as Fig. 8. The track of the eddy from $t = 0$ is shown in each frame.

TABLE 1. Summary of numerical experiments for the triangular jet: ϵ [defined by (13)] is the ratio of the maximum eddy-induced velocity in the jet to the maximum jet velocity. The asterisk indicates that the separation of eddies in the wake could not be determined because it was too variable.

Figure	Γ	$y_p(0)$	ϵ	Eddy drift	Initial condition	Wake eddy period
7	0	—	—	—	most unstable mode	$\lambda_u = 5.1333$
9	−2	−4	.11	NE	$L_j(x, 0) = 0$	$\approx 1.3\lambda_u$
none	−4	−8	.09	NE	$L_j(x, 0) = 0$	$\approx 1.5\lambda_u$
none	−2	−4	.11	E	linear steady solution	$\approx \lambda_u$
10	+2	−3	.16	SW	$L_j(x, 0) = 0$	*
11	−2	−2	.32	NE	$L_j(x, 0) = 0$	*

shows that nonlinearities rapidly destroy this supposedly steady solution and that the wake pattern, while qualitatively similar to that of Fig. 9, contains significant differences. For example, the wake eddy spacing is λ_u. The eddy drifts primarily east, and there appears to be some tendency for the steady solution to persist locally above the eddy.

Increasingly nonlinear interactions starting from a zonal jet (Figs. 10 and 11) suggest that $\partial y_p/\partial t$ and Γ generally remain of opposite sign. When a regular eddy is placed closer to the jet (Fig. 10), it begins to strip off negative potential vorticity from the edge of the jet, and the resulting pair move away from the jet as a vortex dipole. Opposite eddies continue to move toward the jet and eventually (Fig. 11) become incorporated into the wake eddies. Note that the eddy of Fig. 11 is a circular patch of constant vorticity (although a point vortex would behave nearly identically). The effect of replacing a point vortex by a patch will be discussed in section 7.

The parameters used in the numerical experiments on the triangular jet are summarized in Table 1. In conclusion, interactions between an eddy and triangular jet are characterized as follows: the steady-state solution in (18) generally does not form, even locally near the eddy. The location and separation of the wake eddies is quite sensitive to small alterations in the initial state of the jet, and the separation of wake eddies increases as the forcing eddy is moved away from the jet. That the resulting wake is not periodic in x, combined with the long decay scale for the velocity induced by a barotropic eddy, implies that the wake does not drift uniformly downstream and the wake will eventually grossly affect the forcing vortex. The drift tendency for a regular (opposite) eddy interacting with an initially zonal jet is upstream and away from the jet (downstream and toward). In a nonlinear interaction regular eddies tend to strip off potential vorticity from the edge of the jet and move away from it while opposite eddies move into the jet and become incorporated into the wake.

6. The asymmetric equivalent barotropic jet

Our second example is an asymmetric jet used previously for modeling Gulf Stream processes (Pratt et

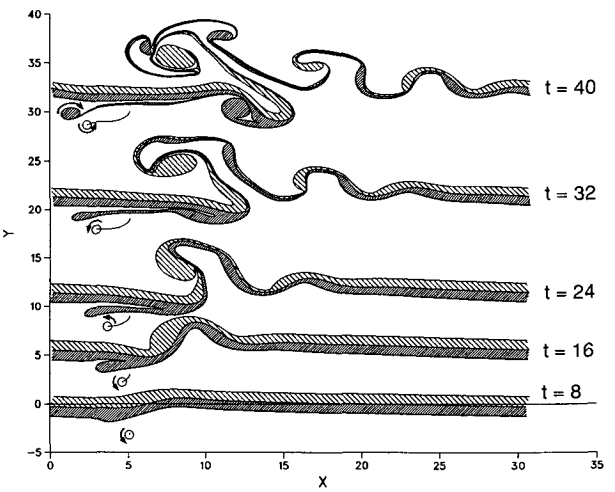

FIG. 10. A regular eddy stripping off an opposite eddy from the edge of the jet ($\Gamma = +2$, $y_p(0) = -3$). Note the track of the eddy, which indicates southwestward propagation.

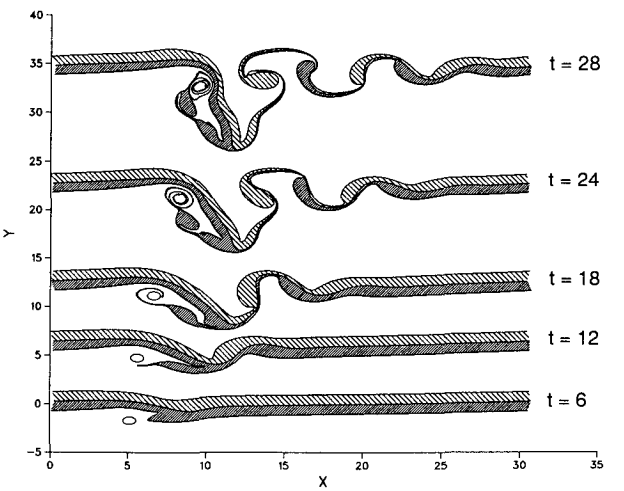

FIG. 11. An opposite eddy is incorporated into the vortex street ($\Gamma = -2$, $y_p(0) = -2$). Initially, the eddy is a circular patch of constant vorticity of radius 0.5.

al. 1990). We use a length scale equal to one deformation radius ($\gamma = 1$) and two contours separated by half a deformation radius. The basic velocity profile $U(y)$ decays by a factor e^{-1} over a deformation radius, and the total width of the undisturbed jet is therefore approximately two and one half deformation radii, or about 100 km (comparable to the Gulf Stream). The parameter r measures the strength of the potential vorticity jump across the southern contour relative to the jump across the northern contour. Observational evidence (Pratt et al. 1990; Hall 1985) suggests a value of $r = 0.3$ to 0.8 for the Gulf Stream. The undisturbed velocity profile is given by (28)

$$U(y) = \frac{1}{2}[e^{-|y|} - re^{-|y+0.5|}]. \qquad (24)$$

Figure 2b shows the velocity profile $U(y)$ for several values of r.

The nonlinear evolution of the flow was calculated numerically by a contour dynamics method (see appendix B). The dispersion relation for the case $r = 0.2$ is shown in Fig. 12. In contrast to the triangular jet of section 5, this jet has a long-wave cutoff and all the unstable waves have relatively large phase velocities. As r increases, the band of unstable waves expands, and when $r = 1$, there is no longer a long-wave cutoff.

Figure 13 shows the evolution of the most unstable mode when $r = 0.2$, given by $\bar{k}_u = 2.1886$. The conservation law (22) (with $\Gamma = 0$) implies that the southern contour will undergo larger deformations than the northern one, even in a nonlinear sense. Indeed, this is the case, and the growing waves in the southern contour eventually break, forming eddies. Pictorially, the break down of this jet is similar to that of the triangular jet (Fig. 7), but the resulting velocity fields are very

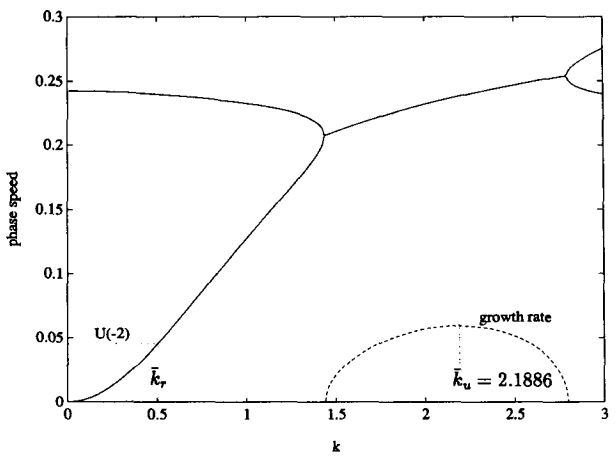

FIG. 12. The dispersion relationship for the equivalent barotropic jet with $r = 0.2$. Here $\bar{k}_u$ is the wavenumber of the fastest growing unstable wave, and $\bar{k}_r$ is the wavenumber of the resonant wave when $y_p(0) = -2$.

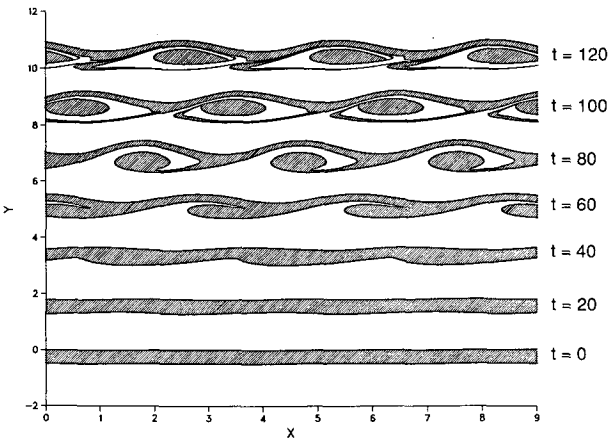

FIG. 13. The nonlinear development of the most unstable wave, $\bar{k}_u = 2.1886$, initial amplitude $|L_1| = 0.005$.

different. Figure 14a shows the velocity field of the triangular jet (Fig. 7, $t = 30$), while Fig. 14b shows the velocity field for the equivalent barotropic jet (Fig. 13, $t = 120$). The triangular jet has broken up into isolated eddies, while the equivalent barotropic jet is changed little from its unperturbed velocity profile, the only noticeable difference being a small amplitude meander at the wavelength of the most unstable mode. The weak influence of the instability on the jet velocity field in Fig. 14b is due to the fact that the total potential vorticity jump across the jet is large (r is small).

Another significant difference between this jet and the triangular jet is that resonant waves are generally present. The eddy drift speed $c = U(y_p(0))$ is given by (24), and is small when the eddy lies more than one deformation radius from the jet. Figure 12 shows that there exist long neutral waves with small phase speeds.

Figure 15 shows the prediction of the linear theory (18) for the Fourier amplitudes of the northern contour, for $r = 0.2$ and $y_p(0) = -2$. There is a resonant wave with $\bar{k}_r = 0.51$ (indicated in Fig. 12). In Fig. 15, the spectrum for $t > 60$ is dominated by two peaks. The resonant mode corresponds to the first peak with k just over $\bar{k}_r = 0.51$. This mode grows linearly with time as predicted by the linear theory. The second peak, with a wavenumber just under $\bar{k}_u$, corresponds to an unstable mode that grows exponentially with time. The shift in these peaks away from $\bar{k}_r$ and $\bar{k}_u$ is due to the fact that the maximum forcing occurs between the peaks, near $k = 0.6$.

Figure 16 shows the fully nonlinear eddy–jet interaction with the same parameters as Fig. 15, calculated by the contour dynamics program. The basic jet instability is triggered, but drifts downstream rapidly and is replaced by a long wavelength meander. The wavelength of this meander is approximately $0.9\bar{\lambda}_r$ (where $\bar{\lambda}_r \approx 12.5$), and its development corresponds to the

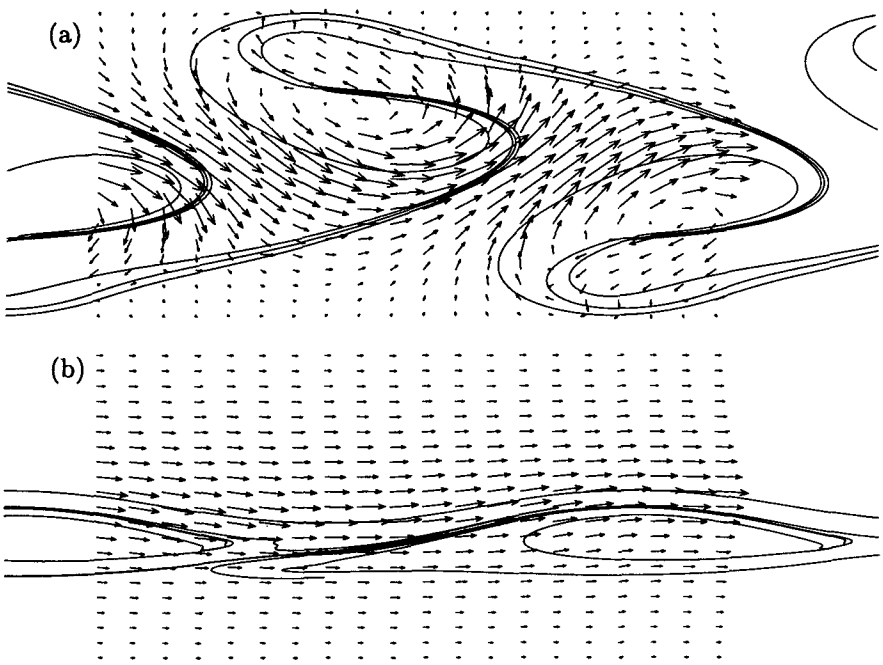

FIG. 14. Velocity fields (in a stationary frame of reference) for the nonlinear development of the most unstable mode for (a) the triangular jet (t = 30, Fig. 7) and (b) the equivalent barotropic jet (t = 120, Fig. 13).

linearly increasing amplitude of the resonant mode in Fig. 15. The relative error (23) between the exact and linear results increases more or less exponentially with time, from 10^{-6} at $t = 0$ to 10^{-2} at $t = 70$.

The wake instability in Fig. 16 is not periodic in x; however, the wake instability continues to drift downstream and essentially exerts no influence on the eddy. This drift is also suggested in the velocity field of the most unstable mode (Fig. 14), which shows that this jet remains more coherent and provides stronger advection. The stagnation point in the flow, indicated by the plus sign (+) in Fig. 16, is well away from the jet, and consequently no stripping occurs.

Starting from $L_j(x, 0) = 0$, the linear theory may be utilized to determine how far the most unstable wave

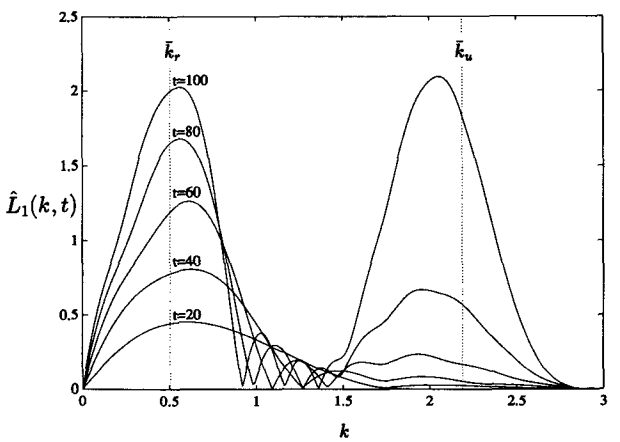

FIG. 15. The linear prediction of $\hat{L}_1(k, t)$, showing a resonant wave growing linearly at $k \approx \bar{k}_r = 0.51$ and an unstable wave growing exponentially at $k \approx \bar{k}_u = 2.1886$.

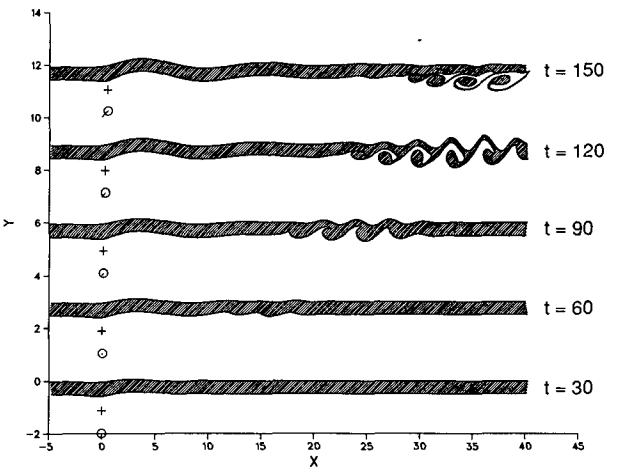

FIG. 16. Weak interaction with $r = 0.2$, $\Gamma = 0.5$, $y_p(0) = -2$, showing the wake instability and steady solution forming behind. Plus sign (+) marks the location of a stagnation point in the flow, in the frame of reference translating with the eddy. The eddy track shows slow northeastward propagation.

has drifted away from the eddy when it reaches finite amplitude. The result of such a calculation is that for $0 < r < \exp(-0.5) \approx 0.6$, in a weak interaction the unstable wave will reach finite amplitude too far from the eddy to influence it. From (21) we may calculate that in this case the direction of meridional eddy drift will be toward the jet for a regular eddy and away from the jet for an opposite eddy. For a jet in the parameter range $r > 0.6$, the unstable wave will grow to finite amplitude near the eddy and will thus dominate its drift.

Figure 16 shows a regular eddy approaching the jet from the south. What is the ultimate fate of such an eddy? According to the weak interaction theory of the previous paragraph it should drift into the jet. As the eddy–jet separation decreases, however, eventually the interaction is no longer weak and linear theory is no longer valid. In Fig. 17 we again begin with an unperturbed jet ($r = 0.5$), but decrease the initial eddy–jet separation from 2 to 1.5. Here the southern contour becomes deformed to a much larger extent than the northern one, and an eddy forms from a pinched off section of the southern contour. In Fig. 17, the eddy and pinched off anticyclonic eddy move southward, away from the jet as a dipole. Southward eddy drift is consistent with (22) because the southern contour is deformed to a much greater extent than the northern one, which is necessary by (22) for southward propagation.

The stagnation point in Fig. 17 (marked by the plus sign) begins inside the jet (Fig. 5a). As the anticyclonic eddy is created from the deformation of the southern contour, the stagnation point moves eastward until it is barely outside the southern contour. When the eddy pinches off, at $t = 24$, the stagnation point moves rapidly westward through the narrowing neck and then southward away from the jet. Using the parameters of Fig. 17, but reversing the sign of Γ, the interaction is much less dramatic (no figure). The eddy does not drift at all meridionally and merely drifts sluggishly eastward.

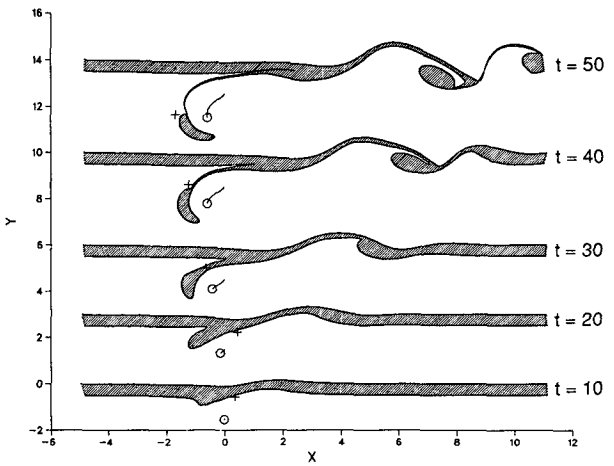

FIG. 17. A regular eddy stripping off an opposite eddy from the south edge of the jet ($r = 0.5$, $\Gamma = 0.75$, $y_p(0) = -1.5$). Plus sign (+) marks the location of a stagnation point in the flow.

When a regular eddy lies to the north of this particular jet, it is not possible for it to strip off an opposite eddy. This is because the vorticity just inside the jet from the northern side is not of the correct sign. Figure 18 shows an anticyclonic eddy (now represented by a patch of constant potential vorticity) approaching the jet from the north. The eddy is drawn in to the jet and incorporated with the anticyclonic eddy that forms due to the basic jet instability.

Table 2 summarizes the parameters used in the numerical simulations of this jet. The numerical results of this section demonstrate that when $\epsilon \ll 1$ and $0 < r < 0.6$, unstable waves drift downstream too quickly to affect the eddy and that a wake of resonant waves will form behind the eddy. Regular (opposite) eddies tend to drift toward (away from) the jet. The wake structure is relatively insensitive to the initial conditions. When a regular eddy approaches a jet, if the near jet edge contains opposite potential vorticity, then the eddy eventually strips an opposite eddy from the edge of the jet and the resulting pair advect one another away from the jet.

7. General eddy–jet interactions

By combining the results of the past two sections with known results on linear jet stability theory, inferences about how an eddy will interact with a general jet may be drawn. We will also discuss the effect of modeling the eddy by a vortex patch rather than a point vortex.

Many of the differences in how our two example jets interact with eddies can be traced back to the differences in the behavior of long wavelength jet perturbations. Drazin and Howard (1962) showed that for a disturbance to a barotropic jet of phase speed ω and wavenumber k, in the limit that $k \to 0$,

$$\omega^2 \sim -\frac{k}{4}\int_{-\infty}^{\infty} [U(y)]^2 dy, \qquad (25)$$

and Flierl (private communication) has proven the same result for a barotropic jet with piecewise constant potential vorticity. According to (25), long waves in a barotropic jet are unstable, and thus, there are no long resonant waves.

The initial meridional drift of an eddy interacting with a zonal barotropic jet is given by (41):

$$\frac{\partial y_p}{\partial t} = -\frac{\Gamma t}{\pi}\int U(y)|y - y_p(0)|^{-3} dy. \qquad (26)$$

Because the integrand in (26) is positive for an eastward jet, the initial meridional eddy propagation tendencies

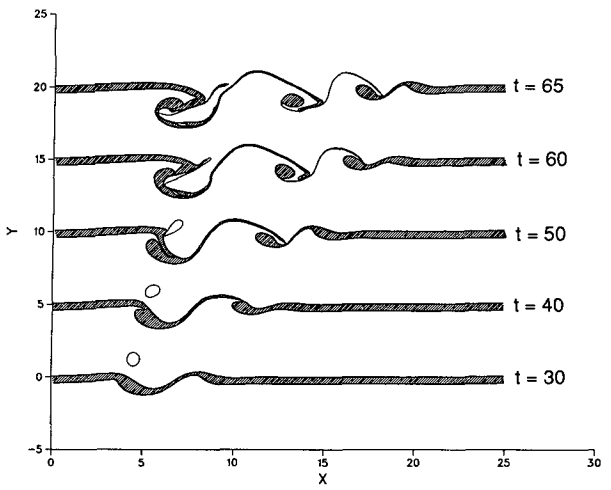

FIG. 18. A regular eddy drifting into the jet from the north ($r = 0.5$, $\Gamma = -0.75$, $y_p(0) = +1.5$). Initially, the eddy is a circular patch of constant potential vorticity of radius 0.4.

for the triangular jet are shared by all barotropic jets. We should note, however, that the meridional drift tendency is very sensitive to the initial jet profile. In general, in a jet where long waves are unstable, the meridional drift of an interacting eddy will eventually be dominated by the nonlinear development of growing unstable waves. Growing unstable waves may break to form eddies, which interact with the forcing eddy, or they may reach finite amplitude in the form of meanders. In the latter case it is the propagation speed of the meander and the phase of the eddy relative to the meander that determines whether or not the eddy–jet separation increases or decreases [a phenomenon discussed by Ikeda and Apel (1990)].

On the other hand, in a jet where long waves are stable, unstable waves may drift downstream rapidly enough that they have no affect on the eddy. Flierl (private communication) has shown that for long waves in an equivalent barotropic jet,

$$\omega \sim k^2 \frac{\int_{-\infty}^{\infty} [U(y)]^2 dy}{\gamma^2 \int_{-\infty}^{\infty} U(y) dy}. \qquad (27)$$

According to (27), long waves are stable and have small phase velocities (when the jet has nonzero net transport). Such long waves are good candidates for resonant waves, and predictable meridional drifting is expected. The direction of meridional drift depends on the form of the resonant wave [by (21)]; however, for the jet considered in section 6 when $r < 0.6$, regular (opposite) eddies tend to drift toward (away from) the jet.

As an eddy nears the jet, clearly it is unrealistic to model it by a point vortex. We repeated all of the calculations in this paper replacing the eddy by a circular patch of radius ρ with the same total circulation. The weak interactions of Figs. 9 and 16 were virtually unchanged over the range $0 \leq \rho \leq 0.7$. Some of the stronger interactions (Figs. 10, 11, 17, and 18) show sensitivity to the value of ρ.

To understand how a circular patch of potential vorticity reacts to the shear of the jet it is useful to recall barotropic studies of a uniform elliptical patch of vorticity ω_0 in a shear flow $U(y) = -sy$, with vorticity s. The work of Moore and Saffman (1971) on steady solutions and Kida (1981) on the dynamics of such vortices concludes the following: an initially circular patch is infinitely elongated by the shear unless $-0.21 < s/\omega_0 < 1$. Thus, a vortex that agrees with the shear remains coherent (is not infinitely elongated) in shears nearly five times as powerful as a vortex that opposes the shear. Recalling the sign of shear that is imposed by the jet upon neighboring vortices, this conclusion may be restated as *regular eddies are much more vulnerable to filamentation as they move into the shear of the jet.*

Our numerical simulations with a circular patch representing the eddy support this statement. Indeed, we did not find a single case of an opposite eddy filamenting or breaking up, even when the eddy was pulled into the jet (Fig. 11), for ρ values up to 0.7. Regular eddies in strong interactions generally filamented or broke up as ρ was increased. In Fig. 18 ($\rho = 0.4$), the eddy merges with one of the eddies formed by the jet instability, and in the process a long filament is pulled off the eddy. If ρ is increased to 0.7, the eddy is rapidly pulled out into a long filament parallel to the jet and does not merge with the jet. Regular eddies involved in the stripping effect (Figs. 10 and 17) also tend to

TABLE 2. Summary of numerical experiments for the asymmetric equivalent barotropic jet. Here ϵ [defined by (13)] is the ratio of the maximum eddy-induced velocity in the jet to the maximum jet velocity.

Figure	r	Γ	$y_p(0)$	ϵ	Eddy drift	Comments
13	0.2	0.	—	—	—	Growth of the most unstable mode
16	0.2	0.5	−2	.05	NE	Resonant wave forms downstream
17	0.5	0.75	−1.5	.21	SW	Negative vorticity fluid stripped off
none	0.5	−0.75	−1.5	.21	E	Surprisingly weak interaction
18	0.5	−0.75	1.5	.10	SE	Eddy pulled into jet

filament as ρ is increased from zero, but the filaments wrap back around the eddy and the stripping phenomena is unchanged. In summary, the only process significantly altered by substituting a distributed eddy for a point vortex is that of a regular eddy moving into the jet. Such an eddy can merge into the jet but only if it is robust enough to survive the shear at the edge of the jet.

8. Discussion

In this paper we have explored weak and strong interactions between an initially zonal, unstable jet and eddy represented by a point vortex. The strength of the interaction is measured by the parameter ϵ, the ratio of the maximum velocity induced by the eddy in the jet to the maximum jet velocity. A weak interaction is by definition an interaction where $\epsilon \ll 1$.

One important conclusion is that the long-wave behavior of a jet greatly influences a weak eddy–jet interaction. If long waves are stable and have small phase speeds, then resonant waves usually exist and the formation of a lee wave results in a meridional drift of the eddy relative to the jet. In the equivalent barotropic jet considered here, regular (opposite) eddies drift toward the jet and downstream (away from the jet and upstream). Shorter wavelength, unstable waves propagate downstream, away from the eddy, and do not significantly influence the eddies position. If long waves are unstable (as in a barotropic jet) then there are no significant resonant waves possible. Meridional drifting may be predicted for a short time after an eddy interacts with an initially zonal jet (and the direction is opposite from that of the equivalent barotropic case), but eventually the effect of finite amplitude unstable waves cannot be ignored.

When the interaction is not weak [$\epsilon = O(1)$], eddy propagation tendencies are more complicated and depend on the specific potential vorticity structure of the jet. One phenomenon that is quite common is the stripping of potential vorticity from the near edge of the jet. Three ingredients appear to ensure that such a stripping process will occur: the forcing eddy must be a regular eddy, the near edge of the jet must contain potential vorticity of opposite sign from the eddy, and a stagnation point must exist in the flow that remains inside the jet for a significant percentage of an eddy turnover time. When these three conditions are met the eddy strips off an opposite eddy from the near jet edge and the resulting pair move upstream and away from the jet. This "vortex stripping" effect has been observed previously in the two-layer primitive equation simulations of Smith and Davis (1989). In the context of a smooth potential vorticity distribution, they demonstrated that this stripping effect may be interpreted as a perturbation in the eddy's azimuthal structure that induces propagation of the regular eddy away from the jet.

Concrete comparisons with observed eddy drift patterns are problematic since a variety of propagation mechanisms are present in geophysical settings. In the Gulf Stream, many rings follow paths that one might anticipate on the basis of recirculation patterns. A 50 Sv (Sv $\equiv 10^6$ m^3 s^{-1}) recirculation distributed over 1-km depth and 1500-km lateral extent would produce a characteristic velocity about 3 cm s^{-1}. This value agrees in magnitude with the advection speed estimates of Halkin and Rossby (1985). In the present 1½-layer model (which seems more applicable to the Gulf Stream than the barotropic model) dimensional propagation speeds can be calculated using the previously defined length and time scales determined by the Rossby deformation radius and maximum jet velocity. For weak interactions (Fig. 16), the typical meridional propagation speed predicted by the linear theory will always be much less than 1 cm s^{-1}, so that we expect the effects of recirculation to dominate. For strong interactions the velocities observed in the numerical experiments (Figs. 17 and 18) range from a few centimeters per second up to 60 cm s^{-1}, so that advection by the recirculation may be secondary. They may be partially valid near 68°–75°W, where Gulf Stream transport reaches a maximum and the meridional velocity due to recirculation is zero.

Another basis for comparison of the 1½-layer model and the Gulf Stream involves warm outbreaks. Pratt et al. (1991) found that outbreaks formed as a result of an instability on the jet side having the weaker potential vorticity jump (the south side) in agreement with the observations of Cornillon et al. (1986). However, the latter also observed that external cold core rings were often involved in the formation process. Here we have shown that regular eddies can, in fact, strip fluid from the southern edge of the jet, creating a mass of detached fluid resembling a warm outbreak (Fig. 17). A corresponding phenomena does not occur at the north edge of the jet. To this extent, theory and observations agree.

A phenomenon observed at the north edge of the Gulf Stream and not present in our model is shingling (the formation of shallow, backward breaking filaments). Shinglelike features have been reproduced in the calculations of Meacham (1991), who considers a jet model similar to that in this paper but with two layers and additional fronts. Shingle formation involves a small-scale shear instability that forms within a relatively narrow potential vorticity band. We anticipate that a similar effect would arise if a third front having relatively weak potential vorticity jump was added a short distance κ to the north of the northern front in Fig. 2b. In this configuration it is unlikely that the shingling process would be strongly influenced by an external eddy since the length scale of eddy forcing would be much greater than the typical wavelength $O(\kappa)$ of the instability. In summary, we believe our

1½-layer model to have insufficient horizontal resolution to display shingling but that, unlike the formation of warm outbreaks, the formation of shingles would be relatively insensitive to the presence of an external eddy.

Acknowledgments. Funding for the publication of this manuscript was provided by the National Science Foundation under Grant OCE 89-16446 and the Office of Naval Research under Grant N00014-89-J-1182. George Bell acknowledges the support received for this research from a postdoctoral fellowship with the Woods Hole Oceanographic Institute. We thank Steven Meacham for his contour dynamics program and the friendly advice that accompanied it.

APPENDIX A

Properties of Weak Eddy–Jet Interactions

1. The basic linear solution

Applying the Fourier transform to (14), we get the system of linear ODEs (17), where

$$\hat{f}_j(k) = \Gamma G_k(a_j - y_p(0))$$

$$A_{jm}(k) = \Delta_m G_k(a_j - a_m) + I_{jm}U(a_j)$$

and where $G_k(y)$ is the Green's function for the operator $\partial^2/\partial y^2 - \gamma^2 - k^2$; that is,

$$\left[\frac{\partial^2}{\partial y^2} - \gamma^2 - k^2\right]G_k(y) = \delta(y).$$

Specifically,

$$G_k(y) = -\frac{1}{2(\gamma^2 + k^2)^{1/2}} \exp[-(\gamma^2 + k^2)^{1/2}|y|].$$

For the triangular jet of section 5, $a_1 = 1$, $a_2 = 0$, $a_3 = -1$, and $\Delta_1 = -1$, $\Delta_2 = 2$, $\Delta_3 = -1$. For the asymmetric equivalent barotropic jet, $a_1 = 0$, $a_2 = -0.5$, and $\Delta_1 = 1$, $\Delta_2 = -r$.

Note, also, that the basic flow $U(y)$ may be represented in terms of the Green's functions $G_k(y)$:

$$U(y) = \begin{cases} -\sum_{j=1}^{n} \Delta_j G_0(y - a_j), & \text{if } \gamma \neq 0 \\ \sum_{j=1}^{n} \Delta_j (y - a_j)H(y - a_j), & \text{if } \gamma = 0. \end{cases} \quad (28)$$

2. The growth of unstable and resonant modes

In this section we begin with the linear solution for the contour displacements in Fourier space (18),

$$\hat{\mathbf{L}}(k, t) = \exp[-ik(\mathbf{A} - c\mathbf{I})t]\hat{\mathbf{L}}(k, 0) + (\mathbf{A} - c\mathbf{I})^{-1} \times \{\mathbf{I} - \exp[-ik(\mathbf{A} - c\mathbf{I})t]\}\hat{\mathbf{f}}(k), \quad (29)$$

and from this derive approximate formulas for the long-term evolution of the contours. Here the exponential of a matrix B is defined as the limit of the series

$$e^{\mathbf{B}} \equiv I + \sum_{j=1}^{\infty} \frac{\mathbf{B}^j}{j!}. \quad (30)$$

We will assume that the nonsymmetric matrix $\mathbf{A} - c\mathbf{I}$ is always diagonalizable, meaning that it may be decomposed as

$$\mathbf{A} - c\mathbf{I} = \mathbf{P}^{-1}\mathbf{D}\mathbf{P},$$

where $\mathbf{P}$ is invertible and $\mathbf{D}$ is a diagonal matrix with diagonal elements equal to the eigenvalues λ_j; that is $D_{ij} = \delta_{ij}\lambda_j$. Note that since $\mathbf{A}$ is a function of k, so are $\mathbf{P}$ and $\mathbf{D}$. For the two cases considered in this paper, $\mathbf{A} - c\mathbf{I}$ is always diagonalizable.

Using the definition of an exponential matrix (30),

$$e^{\alpha(\mathbf{A}-c\mathbf{I})} = \mathbf{P}^{-1}e^{\alpha\mathbf{D}}\mathbf{P}. \quad (31)$$

Applying the identity (31) in (29), we find

$$\hat{\mathbf{L}}(k, t) = \mathbf{P}^{-1}e^{-ik\mathbf{D}t}\mathbf{P}\hat{\mathbf{L}}(k, 0) + \mathbf{P}^{-1}\mathbf{D}^{-1}[\mathbf{I} - e^{-ik\mathbf{D}t}]\mathbf{P}\hat{\mathbf{f}}(k). \quad (32)$$

If k_u is the wavenumber of the fastest growing wave with corresponding eigenvector $\omega(k_u)$ and eigenvector $\mathbf{b}(k_u)$, then it is clear from (32) that for t large

$$\hat{\mathbf{L}}(k_u, t) \propto e^{-ik_u\omega(k_u)t}\mathbf{b}(k_u). \quad (33)$$

A resonant wavenumber k_r, on the other hand, is one for which $\mathbf{A}(k_r)$ has c as an eigenvalue, or $\mathbf{D}$ has a zero diagonal element. In this case $\mathbf{D}$ is not invertible, and (32) must be evaluated with care. By using the definition of the matrix exponential (30) we may rewrite (32) as

$$\hat{\mathbf{L}}(k_r, t) = \mathbf{P}^{-1}e^{-ik_r\mathbf{D}t}\mathbf{P}\hat{\mathbf{L}}(k_r, 0) + ik_rt\hat{\mathbf{f}}(k_r) - \mathbf{P}^{-1}\left[\frac{(-ik_rt)^2\mathbf{D}}{2!} + \frac{(-ik_rt)^3\mathbf{D}^2}{3!} + \cdots\right]\mathbf{P}\hat{\mathbf{f}}(k_r). \quad (34)$$

If there are no unstable waves with wavenumber k_r, then all the elements of $\mathbf{D}$ are real, and the first and third terms on the right-hand side of (34) are bounded. Thus, for t large, only the second term contributes and

$$\hat{\mathbf{L}}(k_r, t) = ik_rt\hat{\mathbf{f}}(k_r). \quad (35)$$

Equation (35) is also the leading-order term in (34) in the case where t is small, $L_j(x, 0) = 0$, and the wavenumber is arbitrary.

3. Linear predictions of meridional eddy drift

The nonlinear expression for meridional eddy drift (22) may be applied to the linear solution (18). In two special cases we can derive analytic expressions for the meridional eddy drift.

First, we can calculate the eddy drift when the jet is stable. In that case, the first two terms in (18) are transients that eventually drift away from the forcing eddy, at which time the solution is well approximated by the steady solution. We now transform this steady solution in (18) back to x. Define $\mathbf{B}(k) \equiv \mathbf{A}(k) - c\mathbf{I}$. Then, formally,

$$\mathbf{B}^{-1} = (\det\mathbf{B})^{-1}(\mathrm{adj}\mathbf{B}),$$

where adj$B$ is the adjoint matrix of B. Inverting the steady solution in (18), we have

$$\mathbf{L}(x) = \frac{1}{2\pi}\int_{-\infty}^{\infty}(\det\mathbf{B})^{-1}(\mathrm{adj}\mathbf{B})\hat{\mathbf{f}}(k)e^{ikx}dk. \quad (36)$$

For large $|x|$, the dominant contribution to the integral in (36) is from the poles where $\det\mathbf{B} = 0$ (note that $\det\mathbf{B}(k_r) = 0$ is the definition of a resonant wavenumber). Since we do not allow waves to enter to the west of the forcing eddy (this is an outgoing radiation condition), we require that $\mathbf{L}(x) = 0$ for $x \ll 0$. Assuming (for simplicity) that there is only one resonant wave at $k = k_r$, then, by the residue theorem for $x \gg 0$,

$$\mathbf{L}(x) \approx -\left\{\left[\frac{\partial(\det\mathbf{B})}{\partial k}\bigg|_{k=k_r}\right]^{-1}(\mathrm{adj}\mathbf{B}(k_r))\hat{\mathbf{f}}(k_r)\right\}\sin k_r x. \quad (37)$$

Now note that by definition

$$\mathbf{B}(k_r)\,\mathrm{adj}\mathbf{B}(k_r) = \det\mathbf{B}(k_r)\mathbf{I} = \mathbf{0}.$$

Therefore, the expression in brackets in (37) is a multiple of the eigenvector $\mathbf{b}$ corresponding to the eigenvalue 0 of $\mathbf{B}(k_r)$. Thus, for $x \gg 0$,

$$\mathbf{L}(x) \propto \mathbf{b}\sin k_r x.$$

If no resonant waves are possible, $\mathbf{L}(x)$ dies out at $x = \pm\infty$; hence, by (22), $\partial y_p/\partial t = 0$. If a resonant wave exists, then a growing wake of resonant waves forms (as in Bell 1990), and $\partial y_p/\partial t \to C$, where C is a constant. The sign of C is determined by the meridional drift implied in (22) for a growing wake of resonant waves; namely,

$$\Gamma\frac{\partial y_p}{\partial t} \propto \sum_{j=1,n}\Delta_j|b_j(k_r)|^2. \quad (38)$$

Surprisingly enough, if the jet is unstable and the unstable waves drift downstream rapidly enough, (38) may still give an accurate estimate of the eddy drift rate.

Second, the eddy drift rate may also be calculated directly by substituting the linear solution (18) into the nonlinear conservation law (22). In the linear theory $|L_j|$ is small, and consequently the integrals in (22) are simply standard integrals over x; by Parseval's relation, (22) becomes

$$\Gamma\frac{\partial y_p}{\partial t} = \frac{1}{4\pi}\frac{\partial}{\partial t}\left\{\sum_{j=1,n}\Delta_j\int_{-\infty}^{\infty}|\hat{L}_j(k,t)|^2dk\right\}. \quad (39)$$

If we substitute in the general linear solution (18), unfortunately the result is an unwieldy expression that can only be evaluated numerically. More specific information can be obtained by assuming that the jet is initially zonal and t is small—in this case the linear solution simplifies to (35). In the barotropic case the integrals in (39) may be evaluated with the result

$$\frac{\partial y_p}{\partial t} = \frac{\Gamma t}{2\pi}\sum_{j=1,n}\Delta_j|a_j - y_p(0)|^{-1}. \quad (40)$$

We may replace the sum in (40) by an integral by substituting $-U''(y)$ for Δ_j and y for a_j. Integrating by parts twice, the boundary terms are zero if the flow is identically zero outside the jet where the eddy is (this is the case for the triangular jet). Thus, (40) may be rewritten

$$\frac{\partial y_p}{\partial t} = -\frac{\Gamma t}{\pi}\int U(y)|y - y_p(0)|^{-3}dy. \quad (41)$$

For an eastward flowing jet, the integrand in (41) is always positive, and consequently, $\partial y_p/\partial t$ and Γ have opposite signs. This result is valid for any eastward-flowing barotropic jet where the flow is identically zero outside the jet.

APPENDIX B

Notes on the Numerical Codes

An extensive literature exists on contour dynamics algorithms (Zabusky et al. 1979; Zabusky and Overman 1981; Pratt and Stern 1986; Polvani 1988). Simple modifications were made to existing programs to produce the output presented here. The parent programs and their modifications are discussed briefly in this appendix.

The nonlinear calculations of section 5, as well as those in section 6 using a circular patch, were produced by a highly recommended two-layer code (Meacham 1991). The computational domain is periodic in x. Nodes were automatically redistributed according to curvature, and contour surgery was not implemented.

The calculations of section 6 using a point vortex were produced by modifying a program used by Pratt et al. (1990). This program is faster than Meacham's, but considerably less general. The stagnation points of Figs. 16 and 17 are roots of the velocity field in the frame of reference translating zonally with the eddy. These roots were found numerically by a secant method for a 2×2 system of equations (see Dahlquist and Bjork 1974).

The area under each jet contour, as well as the total momentum (see Bell and Pratt 1993) were monitored to check the accuracy of the calculation. The initial number of nodes and the time step were adjusted so that these quantities changed less than 1% over the course of a run. In the figures shown herein, initial jet contours contain between 100 and 200 nodes. At the end of the calculation, in some cases, the number of nodes in a contour had increased to nearly 1000.

One advantage of the contour dynamics technique is that it is relatively cheap computationally. Runs in section 5 required an average of 45 minutes CPU time on a Sun Sparkstation, while most runs in section 6 took less than 15 minutes.

REFERENCES

Bell, G. I., 1990: Interaction between vortices and waves in a simple model of geophysical flow. *Phys. Fluids A,* **2,** 575–586.

——, and L. J. Pratt, 1993: Eddy-mean flow interaction theorems for piecewise constant potential vorticity flows. *Dyn. Atmos. Oceans,* submitted.

Cornillon, P., D. Evans, and W. Large, 1986: Warm outbreaks of the Gulf Stream into the Sargasso Sea. *J. Geophys. Res.,* **91,** 6583–6596.

Dahlquist, G. and A. Bjork, 1974: *Numerical Methods.* Prentice-Hall, 570 pp.

Drazin, P. G., and L. N. Howard, 1962: The instability to long waves of unbounded parallel inviscid flow. *J. Fluid Mech.,* **14,** 257–283.

Halkin, D., and T. Rossby, 1985: The structure and transport of the Gulf Stream at 73 W. *J. Phys. Oceanogr.,* **15,** 1439–1452.

Hall, M. M., 1985: Horizontal and vertical structure of velocity, potential vorticity and energy in the Gulf Stream. Ph.D. thesis, MIT/WHOI Joint Program, WHOI-85-16, 165 pp.

Hogg, N. G., and H. M. Stommel, 1985: The heton, an elementary interaction between discrete baroclinic geostrophic vortices, and its implications concerning heat flow. *Proc. Roy. Soc. London,* **A397,** 1–20.

Ikeda, M. and J. R. Apel, 1981: Mesoscale eddies detached from spatially growing meanders in an eastward-flowing oceanic jet using a two-layer quasigeostrophic model. *J. Phys. Oceanogr.,* **11,** 1638–1661.

——, and K. Lygre, 1989: Eddy-current interactions using a two-layer quasigeostropic model. *Mesoscale/Synoptic Coherent Structures in Geophysical Turbulence.* J. C. J. Nihoul and B. M. Jamart, Eds., Elsevier, 277–291.

Kida, S., 1981: Motion of an elliptic vortex in a uniform shear flow. *J. Phys. Soc. Japan,* **50,** 3517–3520.

Meacham, S. P., 1991: Meander evolution on quasigeostrophic jets. *J. Phys. Oceanogr.,* **21,** 1139–1170.

McWilliams, J. C., and G. R. Flierl, 1979: On the evolution of isolated, nonlinear vortices. *J. Phys. Oceanogr.,* **9,** 1155–1182.

Moore, D. W., and P. G. Saffman, 1971: Structure of a line vortex in an imposed strain. *Aircraft Wake Turbulence,* J. H. Olsen and A. Goldburg, Eds., Plenum Press, 339–354.

Nof, D., 1981: On the beta-induced movements of isolated baroclinic eddies. *J. Phys. Oceanogr.,* **11,** 1662–1672.

Polvani, L. M., 1988: Geostrophic vortex dynamics. PhD thesis, MIT/WHOI Joint Program, WHOI-88-48, 221 pp.

——, G. R. Flierl, and N. J. Zabusky, 1989: Filamentation of unstable vortex structures via separatrix crossing: A quantitative estimate of onset time. *Phys. Fluids A,* **1,** 181–184.

Pozrikidis, C., and J. J. L. Higdon, 1987: Instability of compound vortex layers and wakes. *Phys. Fluids,* **30,** 2965–2975.

Pratt, L. J., and M. E. Stern, 1986: Dynamics of potential vorticity fronts and eddy detachment. *J. Phys. Oceanogr.,* **16,** 1101–1120.

——, and J. Pedlosky, 1991: Linear and nonlinear barotropic instability of geostrophic shear layers. *J. Fluid Mech.,* **224,** 49–76.

——, J. Earles, P. Cornillon, and J. F. Cayula, 1990: The nonlinear behavior of varicose disturbance in a simple model of the Gulf Stream. *Deep-Sea Res.,* **38,** S591–S622.

Richardson, P. L., 1983: Gulf Stream rings. *Eddies in Marine Science,* A. R. Robinson, Ed., Springer-Verlag, 19–45.

Smith, D. C., and A. A. Bird, 1989: Factors influencing asymmetry and self advection in ocean eddies. *Mesoscale/Synoptic Coherent Structures in Geophysical Turbulence,* J. C. J. Nihoul and B. M. Jamart, Eds., Elsevier, 211–224.

——, and G. P. Davis, 1989: A numerical study of eddy interaction with an ocean jet. *J. Phys. Oceanogr.,* **19,** 975–986.

Stern, M. E., and G. R. Flierl, 1987: On the interaction of a vortex with a shear flow. *J. Geophys. Res.,* **92,** 10 733–10 744.

Zabusky, N. J., and E. A. Overman, 1981: Regularization of contour dynamical algorithms. *J. Comput. Phys.,* **52,** 357.

——, M. Hughes, and K. V. Roberts, 1979: Contour dynamics for the Euler equations in two dimension. *J. Comput. Phys.,* **30,** 96–106.